Atomic structure of $Al_{89}La_6Ni_5$ metallic glass

2006 J. Phys.: Condens. Matter 18 7579

(http://iopscience.iop.org/0953-8984/18/32/007)

INSTITUTE OF PHYSICS PUBLISHING JOURNAL OF PHYSICS: CONDENSED MATTER

J. Phys.: Condens. Matter **18** (2006) 7579–7592 doi:10.1088/0953-8984/18/32/007

Atomic structure of $Al_{89}La_6Ni_5$ metallic glass

Karel Saksl[1,4], Pál Jóvári[2], Hermann Franz[1], Q S Zeng[3], J F Liu[3] and J Z Jiang[3]

[1] HASYLAB am Deutschen Elektronen Synchrotron, DESY, Notkestrasse 85, D-22603 Hamburg, Germany
[2] Research Institute for Solid State Physics and Optics, Hungarian Academy of Sciences, Budapest, POB 49, H-1525, Hungary
[3] Laboratory of New-Structured Materials, Department of Materials Science and Engineering, Zhejiang University, Hangzhou 310027, People's Republic of China

E-mail: karel.saksl@desy.de

Received 26 May 2006, in final form 28 June 2006
Published 25 July 2006
Online at stacks.iop.org/JPhysCM/18/7579

Abstract

Atomic structures of amorphous $Al_{89}La_6Ni_5$, prepared by single-roller melt spinning, and pre-annealed at 493 and 588 K for 1 h, were characterized by differential scanning calorimetry, x-ray diffraction with a large wavevector transfer value, La L_3-edge and Ni K-edge x-ray absorption fine structure and the reverse Monte Carlo technique. In the as-prepared amorphous alloy, our study reveals that the Ni–Al distance is 2.38 ± 0.02 Å coupled with a coordination number as low as 6.2. The Al–Al distance was found to be ∼4.5% shorter than the nominal atomic diameter of aluminium and the coordination number to be ∼39% less than expected from the dense random packing model. Crystallization of the $Al_{89}La_6Ni_5$ glassy alloy at high temperatures can be described as follows: [amorphous alloy] → [fcc-Al] + [bcc-(AlLa)] + residual amorphous → [fcc-Al] + [o-Al_3Ni] + [o-La_3Al_{11}].

1. Introduction

Al-based amorphous alloys have attracted much attention during the past two decades. Their extraordinary high tensile strength (σ_f more than 1200 MPa) combined with good ductility and low density make Al-based amorphous alloys promising candidates as advanced engineering materials [1–3]. The mechanical properties can even be enhanced (σ_f approaching 1600 MPa) by partially crystallizing the amorphous alloys [4, 5]. The reported mechanical properties of these materials strongly correlate with formation of Al nano-grains and atomic structures at the interfaces between grains and matrix. Thus atomic structure investigations are necessary to understand the mechanical properties and avoid possible pitfalls during the materials design for

[4] Author to whom any correspondence should be addressed.

applications. In our previous work, nucleation of Al nano-grains and high pressure effects on crystallization of $Al_{89}La_6Ni_5$ ternary metallic glass were reported [6, 7]. In this paper we present an atomic structural study on the $Al_{89}La_6Ni_5$ glass by using differential scanning calorimetry (DSC), x-ray powder diffraction (XRD) up to large Q values, La L_3-edge and Ni K-edge extended x-ray absorption fine structure (EXAFS) and reverse Monte Carlo (RMC) techniques. We find that the Ni–Al distance is 2.38 ± 0.02 Å coupled with an average coordination number as low as 6.2 (43% reduction compared to the value derived from the dense random packing (DRP) model), indicating a strong interaction between Ni and Al which corroborates covalent bonding. The Al–Al distance was also found to be ∼4.5% shorter than the nominal atomic diameter of aluminium and the coordination number to be ∼39% less than expected.

2. Experimental details

Ingots, with nominal composition $Al_{89}La_6Ni_5$, were prepared by arc melting a mixture of pure Al (99.99 wt%), La (99.9 wt%), and Ni (above 99.96 wt%) in a purified argon atmosphere. Amorphous ribbons (∼1.3 × 0.02 mm^2) were prepared from the master alloy ingots using a single roller melt-spinning apparatus. Differential scanning calorimetry (DSC) measurements were performed using a Perkin Elmer DSC-7 at a heating rate of 20 K min^{-1}. In order to investigate the structure of the alloy at different stages of crystallization two sets of samples were pre-annealed in vacuum ($<10^{-5}$ mbar) at 493 and 588 K for 1 h. To obtain high resolution radial distribution functions, particularly interesting for atomic structure study of highly disordered materials, XRD data with a large maximum wavevector transfer ($Q = 4\pi \sin\theta/\lambda$) are necessary. Thus, high-energy XRD measurements were performed at HASYLAB at DESY (Hamburg, Germany) on the experimental station PETRA2 using monochromatic synchrotron radiation of 115 keV. The samples measured at room temperature in transmission mode were illuminated for 180 s by a well collimated incident beam of 1 mm^2 cross-section. XRD patterns were recorded using a 2D detector (mar345 Image plate) in asymmetric mode to obtain data at high Q. The background intensity was subtracted directly from the 2D XRD pattern and the result was integrated to Q-space by using the program Fit2D [8]. The integrated data were corrected for polarization, sample absorption, fluorescence contribution and inelastic scattering. The total structural factor $S(Q)$ was obtained by using the Faber–Ziman equation [9]. X-ray absorption fine structure measurements at La L_3 (photon energy 5483 eV) and Ni K (8333 eV) edges were performed at HASYLAB at the experimental station E4. Spectra were collected at room temperature in transmission mode using a fixed exit double-crystal Si(111) monochromator. Experimentally measured x-ray absorption cross sections $\mu(E)$ were analysed by standard procedures of data reduction, using the program Viper [10]. In order to derive quantitative values for the interatomic distances r, coordination numbers N, mean-square relative displacements σ^2 and threshold energy shifts E_0 we carried out a curve fitting analysis of k-space amplitudes and phases.

2.1. Reverse Monte Carlo simulation

The reverse Monte Carlo simulation technique [11–14] is an iterative method for generating large three dimensional models compatible with available structural information (e.g. diffraction or EXAFS measurements). Key parameters of the simulation procedure are the density and the minimum interatomic distances. The density of $Al_{89}La_6Ni_5$ can be estimated in different ways. In the present work we adopted the value reported by Hsieh *et al* (3.21 g cm^{-3} (0.0567 Å^{-3})) for amorphous $Al_{90}Ce_5Fe_5$ [15]. It is to be mentioned that linear combination of

the molar volumes of crystalline phases (fcc-Al, o-Al_3Ni, o-$Al_{11}La_3$) obtained by annealing $Al_{89}La_6Ni_5$ gives 0.0582 $Å^{-3}$. The following minimum interatomic distances were used throughout the simulation runs: Al–Al 2.6 Å, Al–La 3.1 Å, Al–Ni 2.2 Å, La–La 3.0 Å, La–Ni 2.7 Å and Ni–Ni 4.0 Å. Some runs were carried out with larger La–La and La–Ni distances (5.0 and 4.5 Å, respectively). The $g_{AlX}(r)$ (X = Al, La, Ni) functions primarily investigated in this work were not significantly influenced by the choice of these parameters. On the other hand, a better fit could be obtained (especially for the x-ray measurement) by applying the lower La–La and La–Ni distances.

The simulation box contained 20 000 atoms. The length of the box was 70.66 Å, corresponding to a density of 0.0567 $Å^{-3}$. Initial configurations were obtained by hard sphere Monte Carlo runs (satisfying only the above cut-off constraints but fitting no experimental data). The main steps of the reverse Monte Carlo simulation technique can be summarized as follows (for details of the modelling procedure we refer to a recent review [12]).

(1) The partial functions are calculated from the initial atomic coordinates. For diffraction the partial $g_{ij}(r)$ functions are transformed to reciprocal space by the following equation:

$$S_{ij}(Q) = \frac{4\pi\rho}{Q}\int r \sin Qr(g_{ij}(r) - 1)\,\mathrm{d}r \tag{1}$$

where i and j run over the atomic species. ρ is the average number density and r is a distance. The S_{ij} partial structure factors are then combined to $S_m(Q)$, the model reduced x-ray interference function:

$$S_m(Q) = \sum_{ij} w_{ij}(Q)S_{ij}(Q). \tag{2}$$

The w_{ij} weights can be calculated from the $f(Q)$ atomic form factors [16] and compositions in the following way:

$$w_{ij} = \frac{(2 - \delta_{ij})c_i c_j f_i(Q) f_j(Q)}{\sum_{ij} c_i c_j f_i(Q) f_i(Q)}, \tag{3}$$

where c_j is the concentration of the jth atomic species and δ_{ij} represents the Kronecker delta symbol. The model EXAFS signal $\chi_{m,i}(k)$, at the absorption edge of i-type atoms (here La, Ni) can be calculated from the g_{ij} functions via the following equation:

$$\chi_{m,i}(k) - \sum_j 4\pi c_j \rho \int r^2 \gamma_{ij}(r,k) g_{ij}(r)\,\mathrm{d}r. \tag{4}$$

Here γ_{ij} is the backscattering signal of an atomic pair that contains both amplitude and phase information:

$$\gamma_{ij}(r,k) = A_{ij}(k,r)\sin(2kr + \Phi_{ij}(kr)). \tag{5}$$

The A_{ij} amplitudes and Φ_{ij} phase shifts were calculated by the FEFF 8.1 code [17].

Once the model quantities are known their deviation from the experimental ones (denoted by S_{expt}, $\chi_{expt,La}$ and $\chi_{expt,Ni}$) is calculated in the following way:

$$\delta^2 = \frac{1}{\varepsilon^2}\sum_n (S_m(q_n) - S_{expt}(q_n))^2 + \frac{1}{\varepsilon_{La}^2}\sum_n (\chi_{m,La}(k_n) - \chi_{expt,La}(k_n))^2 + \frac{1}{\varepsilon_{Ni}^2}\sum_n (\chi_{m,Ni}(k_n) - \chi_{expt,Ni}(k_n))^2. \tag{6}$$

Here the ε are parameters to regulate the weight of the dataset given in the fitting procedure. (Please note that δ and ε are denoted by χ and σ in the RMC literature. Here δ and ε are used in order to avoid confusion with EXAFS terminology.)

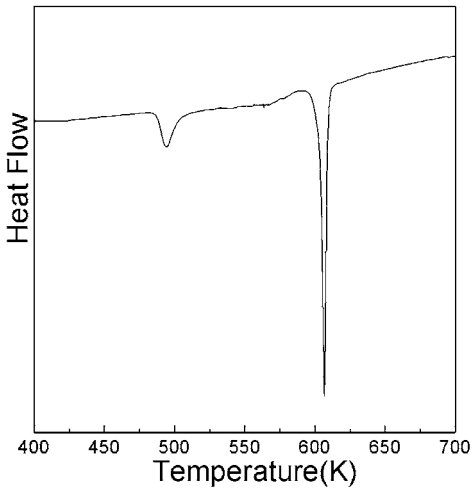

Figure 1. DSC curve of as-prepared $Al_{89}La_6Ni_5$ at a heating rate of 20 K min^{-1}.

(2) One atom is moved randomly and the whole procedure under (1) is repeated to get the δ^2_{new}, the new δ value. The move is accepted if $\delta^2_{new} < \delta^2$, otherwise it is accepted with probability $\exp(-(\delta^2_{new} - \delta^2)/2)$. In a typical RMC simulation run 2 is repeated several million times until the equilibrium is reached and δ^2 starts to oscillate around a constant value.

3. Results

3.1. DSC measurement

The DSC trace of amorphous $Al_{89}La_6Ni_5$ shown in figure 1 exhibits two exothermic heat effects (crystallization peaks) and no glass transition.

XRD experimental results proved that the first exothermic peak around $Tx_1 = 494$ K corresponds to a eutectic crystallization of fcc-Al and bcc-AlLa phases. The second peak at $Tx_2 = 607$ K on the other hand results from the transformation of the residual amorphous component and the metastable bcc crystalline compound to stable orthorhombic Al_3Ni and $Al_{11}La_3$. This crystallization process for the $Al_{89}La_6Ni_5$ alloy is consistent with our previous studies [6] and [7].

3.2. XRD measurements

Figure 2 shows XRD patterns from the as-prepared and pre-annealed samples. The as-prepared sample (despite the low concentration of solute elements (11 at.%)) exhibits the diffuse scattering pattern typical for metallic glasses with a maximum at $Q = 2.6$ Å^{-1} and a pre-peak located at $Q = 1.3$ Å^{-1}. The XRD pattern taken from the pre-annealed alloy at 493 K on the other hand shows distinct Bragg peaks from fcc-Al (marked by asterisks) and bcc-AlLa in addition to the diffuse amorphous contribution. Simultaneous crystallization of the two phases has been ascertained by an *in situ* experiment (not shown here) indicating the eutectic rather than primary nature of the first crystallization. The newly formed bcc-AlLa crystalline phase has peak positions as well as relative peak intensities close to cubic $Al_{92}La_8$ (open triangles, $a = 6.653$ Å) listed in the PCPDFWIN database [18], suggesting a similar

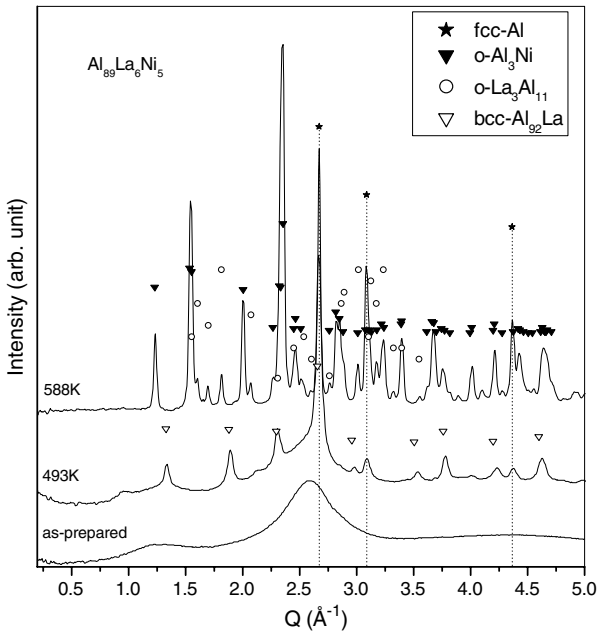

Figure 2. XRD patterns of $Al_{89}La_6Ni_5$ in as-prepared state and pre-annealed at 493 and 588 K.

crystalline structure. EXAFS results (discussed later) also support the idea that the bcc-phase is formed exclusively from Al and La atoms. The mean-square relative displacement value of Al coordinated to La atoms $\sigma^2_{\mathrm{La-Al}}$ after pre-annealing at 493 K is significantly smaller (see table 2) than for the as-prepared stage. On the other hand, for an environment of Ni atoms $\sigma^2_{\mathrm{Ni-Al}}$ values in both samples are very similar. Therefore, one can assume that pronounced changes in the La–Al short-range order are directly connected to the formation of the bcc phase. The XRD pattern from $Al_{89}La_6Ni_5$ pre-annealed at 588 K for 1 h looks fully crystallized and the products of the crystallization were identified as fcc-Al (S.G. $Fm\bar{3}m$; $a = 4.0494$ Å), orthorhombic-Al_3Ni (S.G. $Pnma$; $a = 6.598$ Å, $b = 7.352$ Å, $c = 4.802$ Å) and orthorhombic-La_3Al_{11} (S.G. $Immm$; $a = 4.431$ Å, $b = 10.13$ Å, $c = 13.14$ Å). Schematic drawings of the stable orthorhombic phases are shown in figure 3. Table 1 summarizes the structural parameters (nearest neighbour distances and coordination number) for o-La_3Al_{11} and o-Al_3Ni.

3.3. EXAFS measurements

Figures 4(a) and 5(a) show the absolute values of the Fourier transforms (FTs) of the k^2 weighted EXAFS signals extracted above the La L_3 and Ni K edges, respectively. Closer inspection of figure 4(a) reveals shoulders to the main peaks in the pre-annealed samples. The low r side shoulder is visible on the sample pre-annealed at 493 K, while the high r side can be seen after pre-annealing at the higher temperature.

The calculated Ni K-edge FT signals from the amorphous sample and from the sample annealed at 493 K (shown in figure 5(a)) on the other hand are very similar. The similar FTs obtained from the as-prepared state and after first crystallization suggest a similar atomic arrangement around Ni and have been already discussed in the XRD section of this work. The signal obtained from the sample pre-annealed at 588 K, on the other hand, displays the formation of three distinct coordination spheres (marked by arrows) clearly resulting from

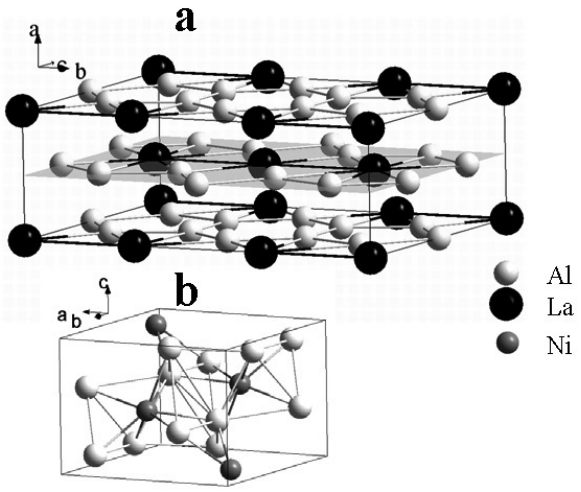

Figure 3. Schematic drawings of (a) orthorhombic-La_3Al_{11}, (b) orthorhombic-Al_3Ni phases.

Table 1. Average pair lengths r_{wa} and coordination numbers N in orthorhombic $Al_{11}La_3$ and Al_3Ni.

Orthorhombic $Al_{11}La_3$		
Pair	r_{wa}	N
La(1)–Al	3.423	16
La(2)–Al	3.365	16
Al(1)–Al	3.029	8
Al(2)–Al	2.652	5
Al(3)–Al	2.789	6
Al(4)–Al	2.796	6
Orthorhombic Al_3Ni		
Ni–Al	2.489	9
Al(1)–Al	2.842	6
Al(2)–Al	2.842	8

formation of Al_3Ni. In order to obtain quantitative values of structural parameters from the first shell around La and Ni absorbing atoms, the shells were first isolated from the rest by applying Hanning windows (1.6–3.7 Å for La and 0.8–2.8 Å for Ni) followed by back Fourier transformation (BFT) to k-space. In the next step the filtered signals were fitted by the EXAFS formula based on the single scattering approximation [19]. During the fitting the following assumptions were made. (a) Both La and Ni atoms are surrounded by Al atoms only. This condition is reasonable taking into account the low atomic concentration of solute elements in the $Al_{89}La_6Ni_5$ alloy. The La and Ni atoms in crystalline $Al_{11}La_3$ and Al_3Ni are surrounded exclusively by Al atoms. Additionally, the structural study on the similar alloys $Al_{87}Ni_7Nd_6$ [20] and $Al_{0.91}La_{0.09}$ [21] documents the first shell coordinating TM and RE atoms consist of Al atoms. (b) Theoretical back-scattering amplitudes and phase shifts were calculated from the orthorhombic atomic configuration, using the FEFF 8.1 code [17]. (c) As a result of the non-Gaussian Al distance distribution around La, a two-shell model was applied to fit corresponding La–Al BFT signals. The use of the two-shell model was primarily verified by

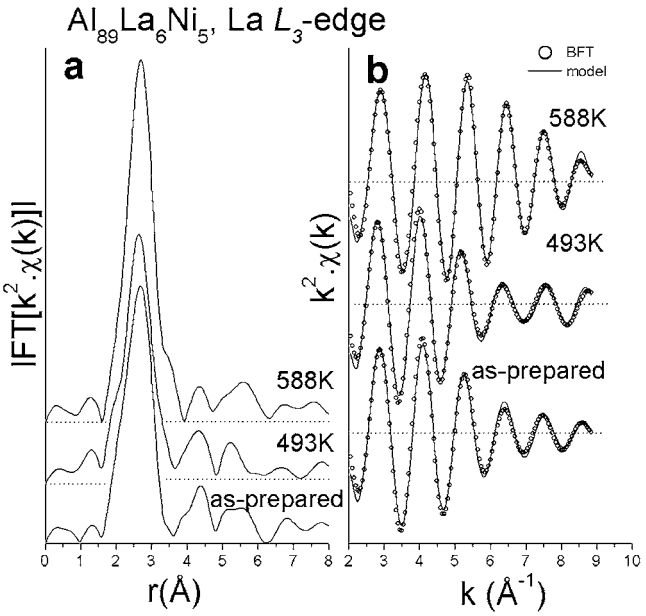

Figure 4. (a) Fourier transforms of experimental $k^2 \cdot \chi(k)$ signals obtained from $Al_{89}La_6Ni_5$ alloy in as-prepared state and after pre-annealing at 493 and 588 K measured above the La L_3 edge. (b) Comparison of filtered and calculated two-shell fits of La L_3-edge EXAFS data using structural data listed in table 2.

Table 2. Structural parameters of amorphous and crystalline $Al_{89}La_6Ni_5$ determined from the La-L_3, Ni-K edge EXAFS spectra analysis; C–B means central–back-scattered atoms. Structural parameters of amorphous $Al_{89}La_6Ni_5$ obtained by RMC simultaneously modelling the x-ray structure factor and the La-L_3, Ni-K edge EXAFS datasets.

EXAFS analysis					
Annealing	C–B pairs	R (Å)	N	σ^2 (Å^2)	ΔE_0 (eV)
As prepared	La–Al(1)	3.28 ± 0.04	12.4 ± 1	0.021 ± 0.002	5 ± 1
Sample	La–Al(2)	3.51 ± 0.08	3.4 ± 1		
	Ni–Al	2.43 ± 0.01	6 ± 0.5	0.0087 ± 0.0014	-2.3 ± 1
493 K	La–Al(1)	3.28 ± 0.03	9.7 ± 1	0.013 ± 0.002	5.6 ± 1
	La–Al(2)	3.52 ± 0.03	7.4 ± 1		
	Ni–Al	2.43 ± 0.01	5.9 ± 0.5	0.0094 ± 0.0014	-2.1 ± 1
588 K	La–Al(1)	3.27 ± 0.02	13.6 ± 1	0.016 ± 0.002	4.8 ± 1
	La–Al(2)	3.70 ± 0.03	3.6 ± 1		
	Ni–Al	2.431 ± 0.008	7.5 ± 1	0.0061 ± 0.001	-2.1 ± 1
RMC					
	Pairs	R (Å)	N	XRD weights (%)	
	Al–Al	2.73 ± 0.02	7.7 ± 0.3	51	
As prepared sample	La–Al	3.29 ± 0.02	15.4 ± 0.5	26	
	Ni–Al	2.38 ± 0.02	6.2 ± 0.3	15	

fitting of the experimental datasets. Application of the two-shell model in the minimization procedure leads to significant reduction of model–data residual. A similar two Al sub-shells

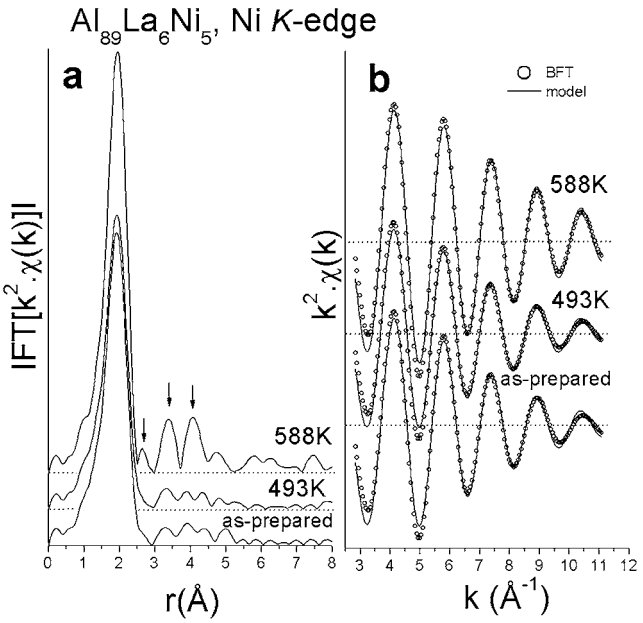

Figure 5. (a) Fourier transforms of experimental $k^2 \cdot \chi(k)$ signals obtained from $Al_{89}La_6Ni_5$ alloy in as-prepared state and after pre-annealing at 493 and 588 K measured above the Ni K edge. (b) Comparison of filtered and calculated single-shell fits of Ni *K*-edge EXAFS data using structural data listed in table 2.

around Nd and Ce were reported for $Al_{87}Ni_7Nd_6$ [20] and ($Al_{80}Co_{10}Ce_{10}$, $Al_{80}Fe_{10}Ce_{10}$) [22], respectively. The first peak of $g_{AlLa}(r)$ obtained by the RMC simulation technique is also strongly asymmetric (see below). During the fitting mean-square relative displacements σ^2 and threshold energy shifts E_0 for both sub-shells were constrained to be equal. In contrast to La, a successful fit of the Ni environment was achieved using a single-shell model only having the parameters unconstrained. Results of numerical fits are listed in table 2. The filtered and calculated EXAFS spectra are shown in figures 4(b) and 5(b). The nearest neighbour distance between La and Al remains unchanged for all samples while the second shell distance only slightly increases with annealing temperature. The weighted average value of the La–Al interatomic distance of 3.33 Å is close to the sum of the nominal atomic radii (3.3 Å) and the coordination number 15.8 obtained from the as-prepared sample is only slightly smaller than the value (17) calculated by the dense random packing (DRP) model using the principle of two-dimensional packing of the atomic surface [23]. The relatively large σ^2_{La-Al} value obtained from the as-prepared sample reflects loosely bound Al atoms in the first coordination shell and significantly decreases after the first crystallization step. A later increase of σ^2_{La-Al} in the sample annealed at 588 K can on the other hand be associated with the formation of the orthorhombic phase. Refined structural parameters from the nearest Al shell coordinating La (listed in table 2) are quantitatively similar to the data reported for the amorphous $Al_{91}La_9$ alloy by Frenkel *et al* [21]. *Important findings of our EXAFS studies are that for the as-prepared sample the Ni–Al interatomic distance is 2.43 Å, about 9% shorter than the sum of nominal atomic radii (2.67 Å). Similarly, the number of Al atoms coordinating Ni is six, which is*∼44%*smaller than the value (10.8) derived on the basis of the DRP model using nominal metallic state radii.* These changes indicate a strong interaction between Ni and Al and suggest covalent bonding of Al to Ni atoms. A similar shortening of interatomic distance coupled with strong reduction of coordination

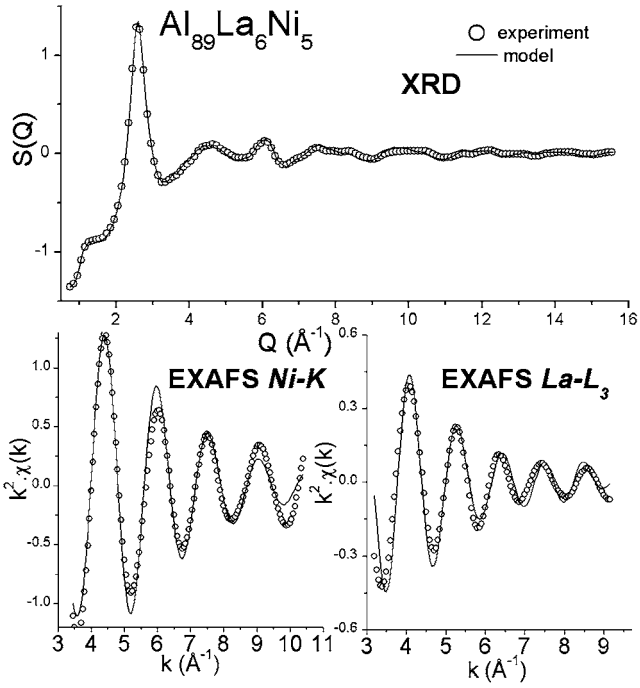

Figure 6. Experimental and RMC modelled XRD reduced interference function, La-L_3 and the Fe K-edge EXAFS signals of amorphous $Al_{89}La_6Ni_5$.

number was reported for amorphous Al–Co–Ce [22], Al–Fe–Ce alloys [22, 24, 15], Al–La–Y [25] $A1_{87}Y_8Ni_5$ and $Al_{90}Y_{10}$ [26] and $Al_{88}Y_7Fe_5$ alloy [27]. This was interpreted to indicate a strong interaction between transition metal and aluminium, corroborating covalent bonding. The σ^2_{Ni-Al} values for as-prepared samples and samples pre-annealed at 493 K are similar and strongly decrease with the formation of Al_3Ni.

3.4. RMC simulation

A favourable property of the EXAFS technique/analysis is its high sensitivity to the environment of the absorbing atoms. This method is, on the other hand, insensitive to medium- and long-range correlations ($\sim$ above 5 Å) and therefore cannot provide a complete overview of atomic structures of the investigated material. An additional limitation of our EXAFS analyses is that in the absence of Al-edge data no information on Al–Al correlations could be obtained. Due to the high percentage of Al the XRD structure factor is most sensitive to Al–Al and Al–La correlations. The combination of EXAFS datasets and the XRD structure factor can therefore offer a more detailed insight into the short-range order of the system investigated. The reverse Monte Carlo (RMC) technique [11–14] provides us with a suitable framework for the simultaneous interpretation of multiple datasets (in general XRD, neutron diffraction and EXAFS). Therefore, we carried out an atomic structure study of as-prepared $Al_{89}La_6Ni_5$ glass by simultaneous RMC modelling of three datasets: the x-ray structure factor and the two EXAFS datasets. Figure 6 shows the comparison of experimental data (open circle) with the simulated data (full line). One can see a very good agreement between experimental and simulated $S(Q)$ while fitting of EXAFS signals results in a small amplitude mismatch,

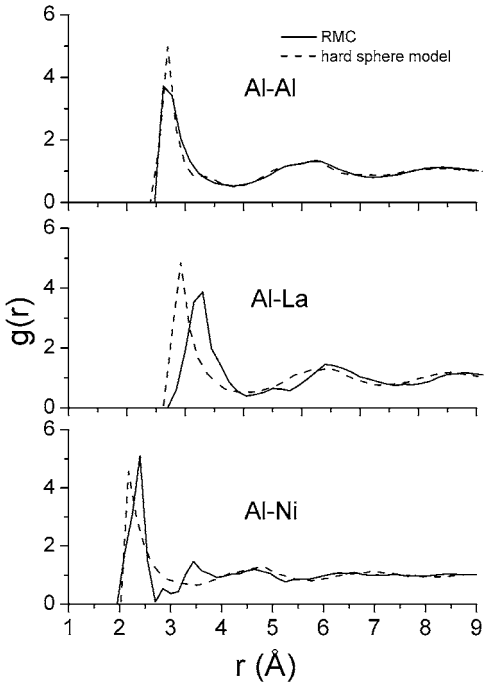

Figure 7. The most dominant partial pair correlation functions $g(r)$, obtained from RMC simulation (solid line) and hard sphere model without fitting of any experimental data (dashed line).

particularly pronounced in the Ni K-edge signal. Figure 7 shows the comparison of most dominant partial pair correlation functions obtained by the RMC simulation.

4. Discussion

4.1. Al–Al pair

Due to large differences in the atomic radii of the constituents ($r_{\mathrm{Al}} = 1.43$ Å, $r_{\mathrm{La}} = 1.87$ Å and $r_{\mathrm{Ni}} = 1.24$ Å) it is possible to separate the first peaks of the Al–Al and Al–La $g(r)$ functions in real space already from the diffraction measurement alone. The peak positions together with corresponding coordination numbers and XRD weights calculated by equation (3) at $Q = 0.75$ Å^{-1} are listed in table 2. The Al–Al mean distance (2.73 Å) is significantly smaller (∼4.5%) than the nominal diameter of an Al atom (2.86 Å).

To check the reliability of the Al–Al peak position, the following should be considered. First, $S_{\mathrm{AlAl}}(Q)$ has the most significant contribution to the x-ray total structure factor (about 30–50%). Second, due to the large separation of the first peaks of the three most significant partial pair correlation functions, $g_{\mathrm{AlAl}}(r)$, $g_{\mathrm{AlLa}}(r)$ and $g_{\mathrm{AlNi}}(r)$, they can be clearly resolved by fitting simultaneously diffraction data with La L_3 and Ni K-edge EXAFS measurements. Regardless of the starting configuration the final Al–Al peak position was always at 2.73 Å. Attempts to move apart Al atoms by raising the minimum Al–Al distance from 2.6 to 2.75 Å resulted in a drastic worsening of the fit of the diffraction data. Thus it can be concluded that the first Al–Al distance is shorter than the nominal diameter of Al atoms. The Al–Al coordination number is 7.7. This is ∼39% smaller than the value of 12.6 calculated by the

DRP model using nominal metallic state radii. It is to be mentioned that a similar contraction of the Al–Al distance was found in crystalline [28, 29] and in quasicrystalline Mg_2Al_3 [29]. *Though there are many studies devoted to the coordination environment of transition metal or lanthanide atoms in Al-based metallic glasses, as far as we know this is the first time that the Al–Al distance and coordination number in an Al-based metallic glass has been determined.*

4.2. Ni–Al and La–Al pairs

The Ni–Al distance (2.39 Å) is significantly shorter than the sum (2.67 Å) of the corresponding atomic radii, and the coordination number obtained (6.2) is also much smaller than the value (10.8) predicted by the DRP model. For La–Al atomic pairs, the first peak is significantly broader, showing a shoulder at high r values. Its shape can be approximated by two Gaussian functions. The weighted average value of the two 'sub-shell' distances is about 3.29 Å, which is very close to the sum of Al and La atomic radii. The La–Al coordination number 15.4 is also close to the value (17) predicted by the DRP model. All structural parameters obtained from RMC simulation (listed in table 2) are in good agreement with corresponding data refined solely from EXAFS signal analysis.

In the case of metallic glasses it is believed that efficient packing plays a key role in the formation of short range order. A simple way of illustrating to what extent the above opinion holds for $Al_{89}La_6Ni_5$ is the comparison of pair correlation functions with those calculated from the initial configuration (obtained by a hard sphere Monte Carlo simulation without fitting any experimental data). Figure 7 shows the Al–X (X = Al, La, Ni) pair correlation functions obtained with the two techniques. It is remarkable that apart from a small peak at about 3.45 Å $g_{AlAl}(r)$ is practically unchanged. The peak at $g_{AlLa}(r)$ is shifted to higher r values and becomes broader if the measurements are simulated. The most drastic changes can be observed in $g_{AlNi}(r)$. As can be expected the first peak is shifted to higher r values and a deep minimum is formed. There is also a pronounced second maximum at about 3.45 Å. It is to be mentioned that though the fine details of these features depend somewhat on the fitting parameters (e.g. the r-range used to calculate the model Ni-edge signal, see equation (4)) the first Ni–Al coordination number and the peak positions are practically model independent.

The transition metal–Al coordination number is close to six in almost every experimental work published on Al–transition metal–rare earth (Al–TM–RE) alloys [15, 22, 24, 26, 27]. As far as we know the only exception is reference [20], where ∼11 was obtained for the Ni–Al coordination number in $Al_{87}Ni_7Nd_6$. Neutron diffraction measurements on isotopically substituted samples are often the most conclusive tools of structural investigations on disordered materials. However, the density used in the above studies was 0.08 $Å^{-3}$, a value ∼40% higher than the density of $Al_{90}Fe_5Ce_5$ (3.21 g cm^{-3} or 0.0567 $Å^{-3}$) reported in [15]. Even the density of pure Al is only 0.060 $Å^{-3}$. The improper choice of density can seriously influence the coordination numbers deduced from experimental results. Therefore in our opinion the Ni–Al coordination number published in [20] should be treated with reservation.

4.3. Prepeak

Prepeaks are usually considered as a clear indication of 'intermediate range order' or the presence of well defined atomic clusters. According to reference [20] the prepeak disappears for $Al_{87}Ni_7Nd_6$ when the strong neutron scatterer ^{58}Ni isotope is replaced by the weaker scatterer ^{60}Ni (neutron scattering lengths are 14.4 and 2.8 fm, respectively). No such effect can be observed upon $^{142}Nd/^{144}Nd$ isotopic substitution (scattering lengths: 7.7 and 2.8 fm). These

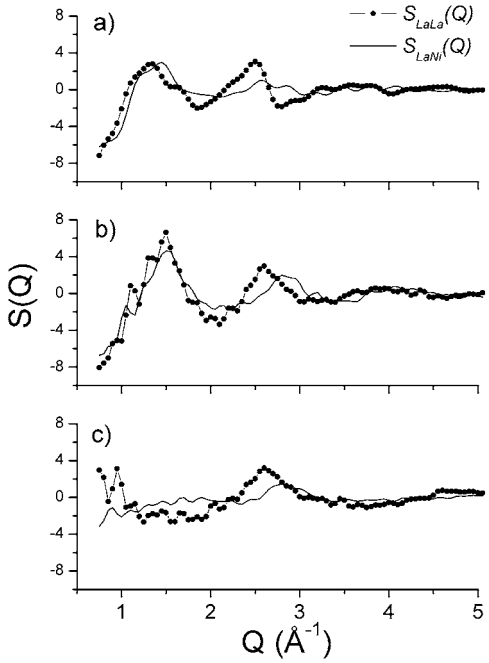

Figure 8. (a) XRD partial structure factors $S_{\mathrm{LaLa}}(Q)$ and $S_{\mathrm{LaNi}}(Q)$ obtained from RMC simulation. (b) The hard sphere Monte Carlo modelling of $S_{\mathrm{LaLa}}(Q)$ and $S_{\mathrm{LaNi}}(Q)$ without fitting of any experimental data; the minimum La–La and La–Ni interatomic distances were set to 4.5 and 5 Å, respectively. (c) The same as (b) but the minimum distance for both was 2.7 Å.

results satisfactorily illustrate the fact that the prepeak is connected with some special ordering of/around Ni atoms and Nd does not contribute to it. In contrast with the above picture, the prepeak was found to be significantly more intense in the case of $Al_{90}Fe_5Ce_5$ than for $Al_{90}Fe_7Ce_3$, where the concentration of transition metal atoms is higher [15]. Moreover, the $S(Q)$ from $Al_{90}Y_{10}$ binary alloy [26] also exhibits a prepeak. This suggests that the Y–Y (or generally RE–RE) correlations contribute to the prepeak, as well. A similar conclusion can be found in our recent XRD study on $Al_{88}Y_7Fe_5$ metallic glass [27].

In order to elucidate the origin of the prepeak we compared $S_{\mathrm{LaLa}}(Q)$ and $S_{\mathrm{LaNi}}(Q)$ partial structure factors calculated by hard sphere Monte Carlo simulations with different minimum interatomic distances (see the reverse Monte Carlo simulation section). When the minimum La–La and La–Ni distances were set to 5.0 and 4.5 Å, respectively, pronounced peaks appear at about 1.5 Å^{-1} on both partial structure factors (figure 8(b)). On the other hand, when the cut-off distances were decreased to 2.7 Å the peaks disappeared (see figure 8(c)). The prepeaks can be found on the partial structure factors from reverse Monte Carlo simulation (figure 8(a)) as well. It should be noted that the quality of the fit improves keeping the lower La–La and La–Ni cut-off distances. The above indicates the presence of a small number of La–La and La–Ni contact pairs in the alloy. Another noticeable fact is that while the sum of the XRD weights of $S_{\mathrm{LaLa}}(Q)$ and $S_{\mathrm{LaNi}}(Q)$ at 1.5 Å^{-1} is 0.088 the weight of $S_{\mathrm{NiNi}}(Q)$ is only 0.008, which means the Ni–Ni pairs have practically negligible contribution to the XRD intensity pattern. The apparent contradiction between reference [20] and our results can be resolved only assuming that the prepeaks in neutron diffraction structure factors are due to TM–TM and TM–RE correlations while prepeaks observed by XRD are from RE–RE and TM–RE partial structure factors.

4.4. Comparison to other literature data

As has been discussed above, some structural aspects of as-prepared $Al_{89}La_6Ni_5$ glass are far from being predicted by the dense random packing model. The Ni–Al and Al–Al interatomic distances are significantly shorter than the sum of the metallic radii and differ also from the corresponding distances in the stable crystalline compound (see table 1). Similar transition metal–Al distance shortening was found in many Al–TM–RE metallic glasses [15, 20, 22, 24, 26, 27]. Up to now, there is no conclusive explanation for this anomalous shortening of the interatomic distances coupled to anomalous coordination number reduction. In case of Ni and Al atomic pairs a strong hybridization of Ni d–Al p states exists, where some 3d localized electrons of Ni atoms and 3p electrons of Al atoms form strong covalent bonds [30]. Based on this knowledge one can presume the existence of small (size beyond the resolution of XRD technique) covalently bound Ni–Al clusters embedded in the amorphous matrix. It is also plausible that due to the strong Ni–Al interaction Al–Al pair distances are reduced in the vicinity of Ni atoms, resulting in smaller average Al–Al distance and coordination number for the as-prepared $Al_{89}La_6Ni_5$. The idea that besides packing considerations the vitrification of metallic melts is facilitated by the formation of well defined and energetically stable structural units is often reported. It is known that some Al-based alloys (e.g. Al–(Pd)–Mn) form icosahedral phases. It is remarkable that the Al–Al distance in liquid $Al_{80}Mn_{20}$ is also significantly shorter than the sum of atomic radii [31]. However, the Ni–Al coordination number found in the present study is much smaller than 12, the coordination number of the central atom of an icosahedron. Therefore, the icosahedral local order around Ni atoms in amorphous $Al_{89}La_6Ni_5$ alloy can be excluded.

It is also to be mentioned that according to a neutron diffraction study [32] the Al–Al distance in icosahedral Al–Fe–Cu is 2.90 Å, suggesting that there is a close relation between local ordering and the nature of chemical interactions between Al–Al and Al–TM pairs.

5. Summary

Atomic structures of amorphous $Al_{89}La_6Ni_5$, prepared by single-roller melt spinning, and pre-annealed samples at 493 and 588 K for 1 h were characterized by x-ray diffraction with a large Q value, La L_3-edge and Ni K-edge x-ray absorption fine structure and reverse Monte Carlo techniques. In the as-prepared amorphous alloy, this reveals an anomalously short Ni–Al distance of 2.38 ± 0.02 Å coupled with an average coordination number close to six. The Al–Al distance was also found to be ∼4.5% shorter than the nominal atomic diameter of aluminium and the coordination number is ∼39% less than expected. On the other hand, the average La–Al distance (3.29 Å) and the average number of Al atoms around La (15.4) both agree reasonably with the values predicted by the DRP model using nominal metallic state radii, which indicate that atomic structure around La atoms in the alloy is most likely similar to the dense random packing model. Crystallization of the $Al_{89}La_6Ni_5$ glassy alloy at high temperatures can be described as follows: [amorphous alloy] → [fcc-Al] + [bcc-(AlLa)] + residual amorphous → [fcc-Al] + [o-Al_3Ni] + [o-La_3Al_{11}].

Acknowledgments

The authors would like to thank HASYLAB staff for support during the experiments. Financial support from the National Natural Science Foundation of China (grant Nos 50341032 and 50425102), the Ministry of Science and Technology of China (grant Nos 2004/249/37-14 and 2004/250/31-01A), the Ministry of Education of China and Zhejiang University is gratefully

acknowledged. PJ was supported by the OTKA (Hungarian Basic Research Fund) grant No T048580.

References

[1] He Y, Poon S J and Shiflet G J 1988 *Science* **241** 1640
[2] Tsai A P, Inoue A and Masumoto T 1988 *Metall. Trans.* A **19** 1369
[3] Inoue A, Matsumoto N and Masumoto T 1990 *Mater. Trans. JIM* **31** 493
[4] Kim Y H, Inoue A and Masumoto T 1990 *Mater. Trans. JIM* **31** 747
[5] Inoue A 1998 *Prog. Mater. Sci.* **43** 365
[6] Zhuang Y X, Jiang J Z, Zhou T J, Rasmussen H, Gerward L, Mezouar M, Crichton W and Inoue A 2000 *Appl. Phys. Lett.* **77** 4133
[7] Zhuang Y X, Jiang J Z, Lin Z G, Mezouar M, Crichton W and Inoue A 2001 *Appl. Phys. Lett.* **79** 743
[8] Hammersley A P, Svensson S O, Hanfland M, Fitch A N and Häusermann D 1996 *High Pressure Res.* **14** 235
[9] Faber T E and Ziman J M 1965 *Phil. Mag.* **11** 153
[10] Klementev K V 2001 *J. Phys. D: Appl. Phys.* **34** 209
[11] McGreevy R L and Pusztai L 1988 *Mol. Simul.* **1** 359
[12] McGreevy R L 2001 *J. Phys.: Condens. Matter* **13** R877
[13] Wicks J D, Börjesson L, Bushnell-Wye G, Howells W S and McGreevy R L 1995 *Phys. Rev. Lett.* **74** 726
[14] Winterer M J 2000 *Appl. Phys.* **88** 5635
[15] Hsieh H Y, Toby B H, Egami T, He Y, Poon S J and Shiflet G J 1990 *J. Mater. Res.* **5** 2807
[16] Waasmaier D and Kirfel A 1995 *Acta Crystallogr.* A **51** 416
[17] Ankudinov A L, Ravel B, Rehr J J and Conradson S D 1998 *Phys. Rev.* B **58** 7565
[18] JCPDS–ICDD. PCPDFWIN, Version 2.0, August 1998: PDF#04-0787 (fcc-Al), #02-0416 (o-Al_3Ni), #24-0501 (o-La_3Al_{11}), and #49-1280 (bcc-$Al_{92}La_8$)
[19] Teo B K 1986 *EXAFS: Basic Principles and Data Analysis* (Berlin: Springer) p 64
[20] Ahn K, Louca D, Poon S J and Shiflet G J 2004 *Phys. Rev.* B **70** 224103
[21] Frenkel A, Stern E A, Voronelm A, Rubshtein A, Ben-Ezra Y and Fleurov V 1996 *Phys. Rev.* B **54** 884
[22] Mansour A N, Wong C P and Brizzolara R A 1994 *Phys. Rev.* B **50** 12401
[23] Egami T and Vitek V 1983 *Amorphous Materials: Modeling of Structure and Properties* (Warrendale PA: TSM-AIME) p 127
[24] Mansour A N, Cibin G, Marcelli A, Sevastyanova T, Yalovega G and Soldatov A V 2001 *J. Synchrotron Radiat.* **8** 809
[25] Yamamoto I, Zytveld J V and Endo H 1996 *J. Non-Cryst. Solids* **205–207** 728
[26] Matsubara E, Waseda Y, Inoue A, Ohtera H and Masumoto T Z 1989 *Naturforsch.* a **44** 814
[27] Saksl K, Jóvári P, Franz H and Jiang J Z 2005 *J. Appl. Phys.* **97** 113507
[28] Samson S 1965 *Acta Crystallogr.* **19** 401
[29] Fournée V, Belin-Ferré E, Sadoc A, Donnadieu P, Flank A M and Müller H 1999 *J. Phys.: Condens. Matter* **11** 191
[30] Xu J, Min B I, Freeman A J and Oguchi T 1990 *Phys. Rev.* B **50** 5010
[31] Maret M, Pasturel A, Senillou C, Dubois J M and Chieux P 1990 *J. Physique* **50** 295
[32] Cornier-Quiquandon M, Quivy A, Lefebvre S, Elkaim E, Heger G, Katz A and Gratias D 1991 *Phys. Rev.* B **44** 2071